

# The efficient sorting of light's orbital angular momentum for optical communications

Martin P. J. Lavery<sup>a</sup>, David Robertson<sup>b</sup>, Mehul Malik<sup>c</sup>, Brandon Rodenburg<sup>c</sup>, Johannes Courtial<sup>a</sup>, Robert W. Boyd<sup>c,d</sup>, and Miles J. Padgett<sup>a</sup>.

<sup>a</sup>School of Physics and Astronomy, University of Glasgow, Glasgow, UK

<sup>b</sup>Centre for Advanced Instrumentation, Department of Physics, Durham University, Durham, DH1 3LE, UK

<sup>c</sup>The Institute of Optics, University of Rochester, 320 Wilmot Bldg, 275 Hutchison Rd, Rochester NY 14627, USA

<sup>d</sup>Department of Physics, University of Ottawa, Ottawa, ON K1N 6N5, Canada

## ABSTRACT

We have developed a mode transformer comprising two custom refractive optical elements which convert orbital angular momentum states into transverse momentum states. This transformation efficiently measures the orbital angular momentum content of an input light beam, allowing the decoding of OAM states within a free-space communications channel. Turbulence is a key issue within such a channel. Through the use of a phase only spatial light modulator, turbulence is simulated, and the cross talk between detected OAM modes is observed. We study this crosstalk for eleven OAM modes, showing that turbulence equally degrades the purity of all the modes within this range.

**Keywords:** orbital angular momentum, turbulence, optical communications

## 1. INTRODUCTION

We are transmitting ever larger amounts of data across optical communications links, and demand is pushing research into many optical properties. One such property is optical orbital angular momentum (OAM).<sup>1</sup> The work by Allen *et al.* in 1992 showed that beams with a transverse complex amplitude profile of the form  $A(r)\exp(i\ell\phi)$  (where  $r$  and  $\phi$  are the radial and angular coordinates, respectively, and  $A(r)$  is the radial part of the amplitude profile) carry an orbital angular momentum of  $\ell\hbar$  per photon.<sup>1,2</sup> An example for such beams are Laguerre-Gaussian (LG) modes, which have a helical phase structure. The integer  $\ell$  is unbounded, giving a large state space in which to encode information.<sup>3-8</sup>

The use of diffractive optical elements (DOEs) containing an  $\ell$ -fold fork dislocation has become commonplace for the generation of beams carrying OAM.<sup>9,10</sup> The forked diffraction grating, when illuminated with a Gaussian beam, for example from a single-mode fibre, produces the helical mode in the first diffraction order. This grating can also be used in reverse to couple light with a helical phase into a single-mode fibre, to measure the power in that mode.<sup>11</sup> Sequentially changing the number of dislocations in the fork allows a range of  $\ell$  values to be measured, but checking for  $N$  states require at least  $N$  photons.<sup>11</sup> Similar techniques have been demonstrated using spiral phase plates and q-plate technology in place of the DOE.<sup>12,13</sup> A method to route OAM at the single photon level was demonstrated by Leach *et al.* It required  $N - 1$  Mach-Zehnder interferometers with a Dove prism in each arm<sup>14,15</sup> for the routing of  $N$  states. In principle, this routing can be achieved with 100% efficiency and with no loss of the input beam's mode structure. However, simultaneously maintaining the alignment of  $N$  interferometers has proved technically challenging.

We previously showed that two phase-only diffractive elements can be used to transform OAM states into transverse momentum states.<sup>16</sup> This was achieved through the use of mapping of a position  $(x, y)$  in the input

---

Further author information: (Send correspondence to M.P.J.L.)  
M.P.J.L.: E-mail: m.lavery.1@research.gla.ac.uk

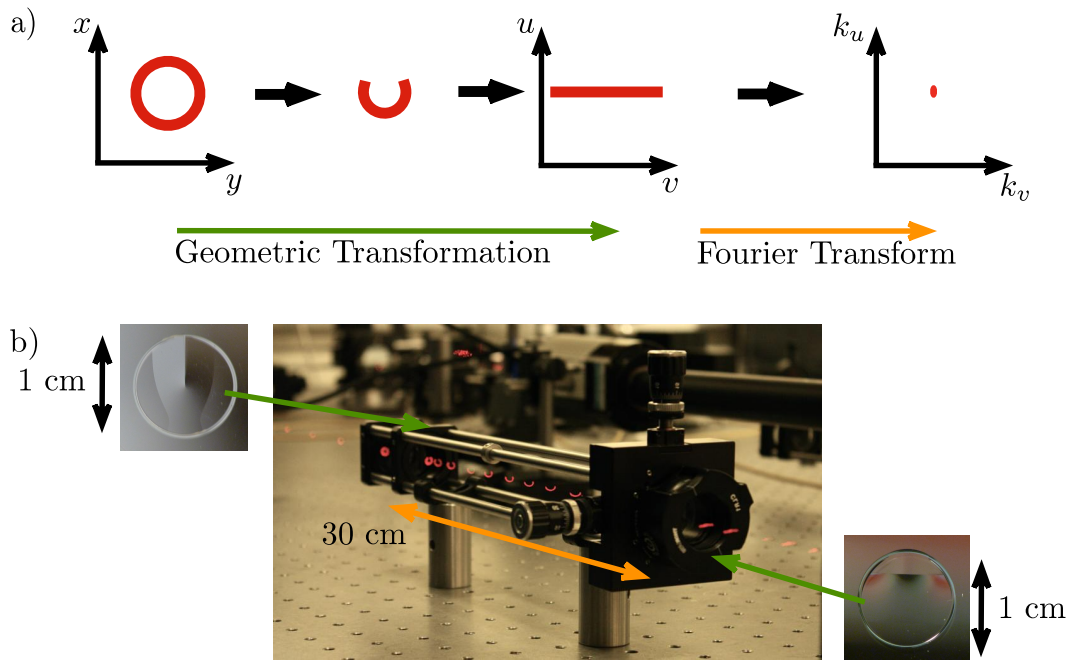


Figure 1. (a) Conversion of OAM states into transverse momentum states with refractive optical elements. An image of the beam was captured in several transverse planes and overlaid (in red) to give the image shown above. (b) A beam carrying OAM is prepared through the use of a  $\ell$ -forked hologram, realised using a spatial light modulator (SLM) and then passed through the two elements, represented as the green rectangle, required to perform the transformation of both the phase and intensity of the beam.

plane to a position  $(u, v)$  in the output plane, where  $u = -a \ln(\sqrt{x^2 + y^2}/b)$  and  $v = a \arctan(y/x)$ .<sup>17–19</sup> A set of concentric rings in the input plane is transformed into a set of parallel lines in the output plane, but the combination of the two diffractive optical elements transforms not only the intensity of the beam but also its phase: the azimuthal phase term  $\exp(i\ell\phi)$  in the input plane becomes, in the output plane,  $\exp(i\ell v/a)$ , i.e. the beam now has a transverse momentum  $\hbar\ell/a$  in the  $v$  direction. A lens can then separate the resulting transverse momentum states into specified lateral positions, allowing for the efficient measurement of multiple states simultaneously.<sup>20, 21</sup>

Separating OAM states in this way presents an opportunity for this larger alphabet to improve the data capacity of a communications link and has potential applications both in the classical and quantum regime. For example, in free-space communications links the use of an alphabet of OAM could present advantages over other encoding techniques.<sup>5, 22</sup> However, the natural random time-dependent variations in temperature and pressure of the atmosphere result in changes in density of the atmosphere, which in turn give a spatially-dependent change of the refractive index, leading to a phase distortion across a transmitted beam. A phase distortion of this type can be approximated to a phase screen, and is commonly referred to as thin phase turbulence.<sup>23</sup> Such a phase distortion is a concern for any free space communications channel where the atmospheric turbulence may affect the cross-talk between channels, an important consideration in any communication system.

We use two bespoke refractive elements which carry out the optical transformation described above (Fig.1). Hence the elements can be used as a decoder for information encoded with OAM states.<sup>24</sup> We then use these elements to experimentally study the effects of atmospheric turbulence on a communications system utilising OAM modes as the information carrier.<sup>25</sup>

The height profiles for the refractive elements were derived from the equations defining the phase profile of the diffractive elements presented in our earlier work,<sup>16</sup> along with the addition of a lens term, indicated in equations (1) and (2) shown below. When light of a particular wavelength,  $\lambda$ , passes through a material of height  $Z$  and with a refractive index  $n$ , the effective optical path length changes with respect to the same distance of propagation in a vacuum. The change in path length can be expressed as a change in phase of

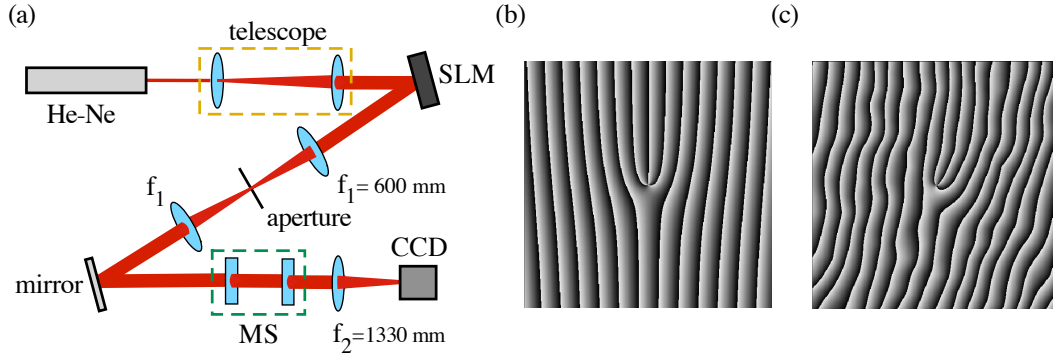


Figure 2. (a) A beam carrying OAM is prepared through the use of a  $\ell$ -forked hologram, seen in (b), realised using a spatial light modulator (SLM), illuminated by an expanded He-Ne laser. The first order beam is imaged onto the front aperture of a OAM mode sorter (MS) which converts OAM states into transverse momentum states with the use of two refractive optical elements. These transverse momentum states are then focused to specific spatial locations on a CCD. The power measured in each of these locations gives a measure of the OAM superposition incident on the mode sorter. (c) Thin phase turbulence is added to the  $\ell$ -forked hologram changing the OAM superposition measured by the system.

$\Delta\Phi = 2\pi(n-1)Z/\lambda$ , hence the first element requires a height profile of

$$Z_1(x, y) = \frac{a}{f(n-1)} \left[ y \arctan\left(\frac{y}{x}\right) - x \ln\left(\frac{\sqrt{x^2 + y^2}}{b}\right) + x - \underbrace{\frac{1}{a}\left(\frac{1}{2}(x^2 + y^2)\right)}_{\text{lens term}} \right], \quad (1)$$

where  $f$  is the focal length of the integrated lens. There are two free parameters,  $a$  and  $b$ , which determine the scaling and position of the transformed beam. The parameter  $a$  takes the value  $a = d/2\pi$ , ensuring that the azimuthal angle range ( $0 \mapsto 2\pi$ ) is mapped onto the full width of the second element,  $d = 8\text{mm}$ . The parameter  $b$  is optimised for the particular physical dimensions of the sorter. The second of these elements has a height profile

$$Z_2(x, y) = -\frac{ab}{f(n-1)} \left[ \exp\left(-\frac{u}{a}\right) \cos\left(\frac{v}{a}\right) - \frac{1}{ab} \underbrace{\left(\frac{1}{2}(x^2 + y^2)\right)}_{\text{lens term}} \right], \quad (2)$$

where  $u$  and  $v$  are the coordinates in the output plane. This element is placed a distance  $f$  behind the first element. Each surface is wavelength independent, but dispersion effects in the material manifest themselves as a change in the focal length of the integrated lens for different wavelengths. Hence, the system can be tuned to a specific wavelength by slightly changing the distance between the elements.

In our experiment we generate Laguerre-Gaussian (LG) beams by expanding a HeNe laser onto an  $\ell$ -forked hologram (Fig. 2(b)), realised using an SLM, by programming the SLM with both phase and intensity information. The beam generated in the first order of the hologram was selected with an aperture and the plane of the SLM is imaged onto the plane of the first element. The beam is then passed through the elements transforming it into the form  $\exp(i\ell v/a)$ , giving a transverse direction state which is then focussed into an elongated spot on a camera. The transverse position of the spot is dependent on  $\ell$ .

Our transformation from orbital angular momentum states into transverse momentum states gives rise to inherent cross talk due to the diffraction limit. The inherent degree of cross talk can be deduced from Fourier theory, which predicts approximately 80% of the input light will be present in the bin corresponding to the input OAM mode value. To experimentally assess the inherent crosstalk of the system, a camera was partitioned into  $N$  adjacent regions, where each region was centred on one of the elongated spots that correspond to a particular value of  $\ell$ , and the measured intensity of the pixels in the region was summed for each region. For a single input

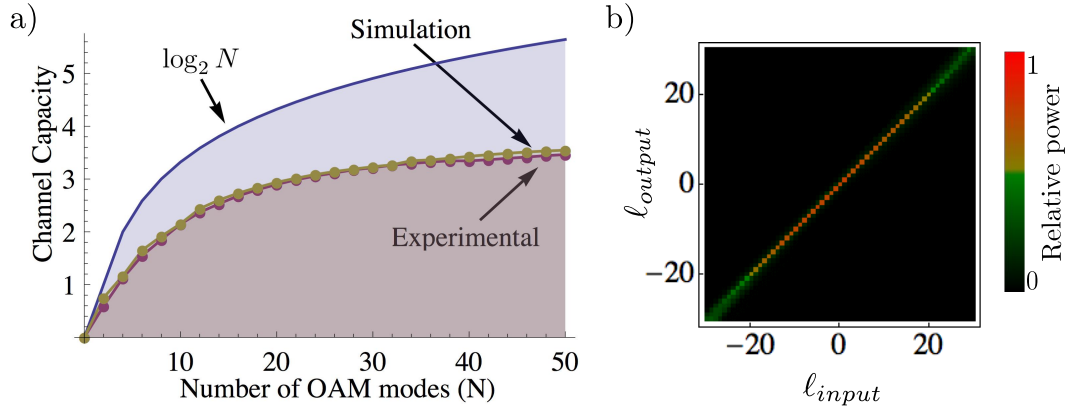


Figure 3. (a) Channel capacity for a  $N$  of LG modes, where  $N = 2, 4, 6, \dots, 50$ . Detector noise was measured with no light incident on the camera, which was overcome by setting a threshold with a signal to noise ratio of 3000 to 1. (b) The ratio of energy measured in each of the detector regions showing the degree of cross talk.

mode, one would expect/hope for the majority of the energy to be detected in the bin corresponding to the input mode; any energy readings in other regions represent cross talk between channels. A common method of evaluating the degree of cross talk in a communications system is the channel capacity, which is the maximum amount of information that can be reliably transmitted by an information carrier.<sup>29</sup> In a multi-channel system, a photon can be in one of  $N$  input states and the maximum channel capacity value is  $\log_2 N$  bits per photon.

To evaluate the range of modes the system is able to detect efficiently, the system is tested using LG beams over the mode range  $\ell = -25$  to  $\ell = +25$ . LG modes were specifically chosen to allow precise control of the beam waist, and for the experimental result to be most closely matched to our numerical modelling of the system. The channel capacity was measured for  $N$  modes, where  $N = 2, 4, 6, \dots, 50$ . For each measurement, the range  $\ell = -N/2$  to  $\ell = N/2$  was used while leaving  $\ell = 0$  free as an alignment channel. The values measured are shown in Fig. 3.

The optical transformation we utilise is only perfect for rays which are normally incident on the transformation elements. Light carrying OAM, such as LG modes, is inherently not of this type as the rays have a skew angle of  $\theta_s = \ell/kr$ , where  $k$  is the wavenumber of the light and  $r$  is the distance from the mode's centre.<sup>30,31</sup> A numerical simulation of the experimental setup was carried out using plane wave decomposition.<sup>16</sup> Comparing channel capacity values from the simulated and experimentally obtained results with that of the maximum possible channel capacity, one sees the difference increase at higher mode ranges. Such results are consistent with the larger skew angles at higher  $\ell$  causing errors in the transformation, hence increasing the channel cross talk at these  $\ell$  values. Our simulations show that a reduction in crosstalk at higher  $\ell$  values can be achieved by an increase in separation between the components or an increase in the aperture size of the system. A study of this effect has recently been submitted.<sup>32</sup>

We introduce precisely simulated amounts of thin phase turbulence through the use of a phase only spatial light modulator. Once the turbulence is introduced, we can measure the resulting cross talk between OAM modes and relate this to atmospheric conditions. The phase screen corresponding to a particular turbulence strength is generated by considering Kolmogorov turbulence theory.<sup>27</sup> The aberrations introduced by atmospheric turbulence can be considered as normal random variables, where the ensemble average can be written as  $\langle [\phi(\mathbf{r}_1) - \phi(\mathbf{r}_2)]^2 \rangle$  and is known as the phase structure function.<sup>26</sup>  $\phi(\mathbf{r}_1)$  and  $\phi(\mathbf{r}_2)$  are two randomly generated phase fluctuations. From Kolmogorov statistics it can be shown that this ensemble average must meet the requirement that

$$\langle [\phi(\mathbf{r}_1) - \phi(\mathbf{r}_2)]^2 \rangle = 6.88 \left| \frac{\mathbf{r}_1 - \mathbf{r}_2}{r_0} \right|^{5/3}. \quad (3)$$

The value  $r_0$  is the Fried parameter, and is a measure of the transverse distance scale over which the refractive index is correlated.<sup>27</sup> To characterise the effect of turbulence on the optical system, a ratio  $D/r_0$  is considered,

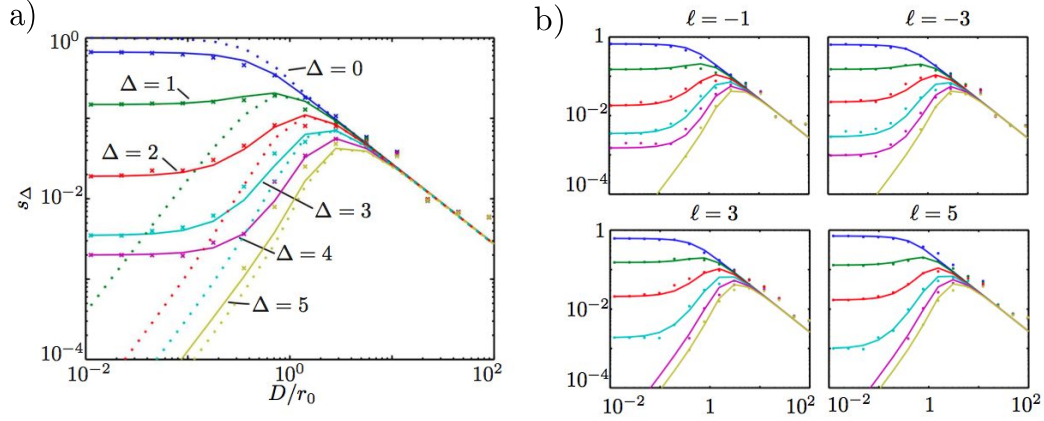


Figure 4. Power,  $s_\Delta$ , in modes with indices  $\ell + \Delta$ , after an incident mode with index  $\ell$  has been propagating through a range of turbulent phase screens with strength characterised by  $D/r_0$ . (a)  $\ell = 0$ ; (b) other values of  $\ell$ . For each experimentally measured value of  $D/r_0$ , denoted as crosses, the measured power in each detected mode was averaged over 100 randomly generated phase screens. These modal powers were then co-plotted against the theoretical predictions given by equation 4, shown as lines.

where  $D$  is the aperture of the system. This ratio sets two limiting cases: in the first case, when  $D/r_0 < 1$ , the resolution of the system is limited by its aperture; in the second case, when  $D/r_0 > 1$ , the atmosphere limits the system's ability to resolve an object.<sup>27</sup>

In 2005, Paterson predicted the spread in the OAM spectrum resulting from thin phase turbulence.<sup>23</sup> For a single OAM mode with index  $\ell$ , transmitted through an ensemble average of many turbulent phase screens, the power,  $s_\Delta$ , in a particular mode with index  $\ell + \Delta$  ( $\Delta = 0, \pm 1, \pm 2, \dots$ ) is given by

$$s_\Delta = \frac{1}{\pi} \int_0^1 \rho d\rho \int_0^{2\pi} d\theta e^{-3.44 \left[ \left( \frac{D}{r_0} \right) \left( \rho \sin \frac{\theta}{2} \right) \right]^{5/3}} \cos \Delta \theta, \quad (4)$$

where  $\rho = 2r/D$ .<sup>26</sup>

Rather than producing a pure Laguerre-Gaussian mode, we produce helically phased modes where the radius of the mode is specifically controlled and the plane of the SLM then imaged, giving a near Gaussian intensity distribution. This approach maintains the ratio  $D/r_0$  independent of the mode index. A particular turbulent phase screen can then be added to this hologram to simulate the presence of atmospheric turbulence. The SLM is then imaged to the 8 mm diameter input pupil of the OAM mode sorter to decompose the resulting beam into its constituent OAM modes.

To measure the effect of turbulence on the channel cross talk, we consider a smaller mode range of  $\ell = -5$  to  $\ell = +5$ . We consider 24 different values of  $D/r_0$ ; for each value, 100 randomly generated phase screens are applied to the input mode and the OAM spectrum was measured (Fig. 4). The power was measured across all the 11 regions and normalised with respect to the power measured for  $\ell = 0$  with no turbulence applied. The measured power was then plotted as a function of the turbulence strength,  $D/r_0$ . As predicted by equation (4), the crosstalk between OAM modes increases with turbulence and in this mid/high turbulence regime we find the agreement between theory and our measurements is good. In the low turbulence regime, the cross-talk between modes arises from residual crosstalk in our mode sorter, which in turn arises from the diffraction limit.<sup>16,24</sup> The weightings of the known input states can be described by an  $N = 11$  element column vector,  $(I_0, I_1, \dots)^T$ . These are mapped by an  $N \times N$  cross-talk matrix onto the measured  $N$ -element output vector  $(O_0, O_1, \dots)^T$ :

$$\begin{bmatrix} O_0 \\ O_1 \\ \vdots \\ O_N \end{bmatrix} = \begin{bmatrix} 1-g & a & \dots & b \\ c & 1-h & \dots & d \\ \dots & \dots & \dots & \dots \\ e & f & \dots & \dots \end{bmatrix} \begin{bmatrix} I_0 \\ I_1 \\ \vdots \\ I_N \end{bmatrix}. \quad (5)$$

For the case of zero residual crosstalk, this matrix would have a leading diagonal of 1's and 0's elsewhere. For finite crosstalk, the coefficients of the crosstalk matrix are measured at zero turbulence and then this matrix is used to predict the measured OAM output spectrum for an input OAM state subject to the atmospheric cross-talk from the Paterson model (Eqn (4)).

It is seen in Fig. 4 that, at high turbulence values, where  $D/r_0 \gg 1$ , the average power is spread between all the possible detections modes. It should be noted that we are only considering the proportion of the power detected within the detector regions and not considering the power incident outside our detectors.

Paterson's earlier work indicates that the probability of modal cross talk resulting from atmospheric turbulence is independent of the mode propagating through that turbulence. For each of these OAM modes in the range from  $\ell = -5$  to  $\ell = +5$ , the same set of turbulent phase screens was applied, and cross-talk measured (Fig. 4(b)). We note that the observed cross-talk is indeed similar for the range of OAM modes we examine.

In this work we have studied the case where turbulence can be considered as thin phase screen. Such an approach is widely used in astronomy, as when one considers the distance to an astronomical light source, the largest proportion of the turbulence is experienced, relatively, very close to the observer. In the case of long distance point to point communications on earth, turbulence is characterised more accurately by multi-plane turbulence, however, we expect similar principles to apply in the two cases.

In conclusion, we have presented a method utilising bespoke optical elements to sort OAM for a wide mode range. We have studied the effect of turbulence on an optical communications channel that uses an OAM-based alphabet. The effects of turbulence were experimentally shown to be independent of mode number and hence a well known turbulence mitigation systems could be implemented to preserve the integrity of the communications link. Such an optical communications link could be attractive to both classical and quantum optical systems.

We acknowledge Dan Gauthier, and Jonathan Leach for helpful discussions. Our work was primarily supported the DARPA InPho program through the US Army Research Office award W911NF-10-1-0395 and the EPSRC. MPJL was further supported by European collaboration EC FP7 255914, PHORBITECH, and M. J. P. is supported by the Royal Society.

## REFERENCES

1. L. Allen, M. Beijersbergen, R. Spreeuw, and J. Woerdman, "Orbital angular momentum of light and the transformation of Laguerre-Gaussian laser modes," *Phys. Rev. A* **45**, 8185–8189 (1992).
2. A. M. Yao, M. J. Padgett, "Orbital angular momentum: origins, behavior and applications", *Adv. Opt. Photon.* **3**, 161-204 (2011).
3. G. Molina-Terriza, J. P. Torres and L. Torner, "Twisted Photons", *Phys. Rev. Lett.* **88**, 013601 (2001).
4. A. Vaziri, G. Weihs and A. Zeilinger, "Experimental Two-Photon, Three-Dimensional Entanglement for Quantum Communication", *Phys. Rev. Lett.* **89**, 240401 (2002).
5. G. Gibson, J. Courtial, M. Padgett, M. Vasnetsov, V. Pas'ko, S. Barnett, and S. Franke-Arnold, "Free-space information transfer using light beams carrying orbital angular momentum," *Opt. Express* **12**, 5448–5456 (2004).
6. J. T. Barreiro, T. C. Wei and P. G. Kwiat, "Beating the channel capacity limit for linear photonic superdense coding" *Nat. Phys.* **4**, 282 (2008).
7. J. Leach *et al.*, "Quantum Correlations in Optical Angle-Orbital Angular Momentum Variables", *Science* **329**, 662 (2010).
8. M. Malik, M. O'Sullivan, B. Rodenburg, M. Mirhosseini, J. Leach, M. P. J. Lavery, M. J. Padgett, and R. W. Boyd, "Influence of atmospheric turbulence on optical communications using orbital angular momentum for encoding", *Opt. Express* **20** 12, 1319513200, 2012.
9. V. Bazhenov, M. Soskin, and M. Vasnetsov, "Screw dislocations in light wave-fronts," *J. Mod. Opt.* **39**, 985–990 (1992).
10. N. Heckenberg, R. McDuff, C. Smith, and A. White, "Generation of optical phase singularities by computer-generated holograms," *Opt. Lett.*, **17** 221–223 (1992).
11. A. Mair, A. Vaziri, G. Weihs, and A. Zeilinger, "Entanglement of the orbital angular momentum states of photons," *Nature* **412**, 313–316, (2001).

12. S. S. Oemrawsingh, J. de Jong, X. Ma and A. Aiello. "High- dimensional mode analyzers for spatial quantum entanglement, *Phys. Rev. A* **73**, 032339, (2006)
13. L. Marrucci, E. Karimi, S. Slussarenko, B. Piccirillo, E. Santamato, E. Nagali and F. Sciarrino, "Spin-to-orbital conversion of the angular momentum of light and its classical and quantum applications", *J. Opt.* **13**, 064001, (2011).
14. J. Leach, M. Padgett, S. Barnett, S. Franke-Arnold, and J. Courtial, "Measuring the orbital angular momentum of a single photon," *Phys. Rev. Lett.* **88**, 25, 257901 (2002).
15. M. P. J. Lavery, A. Dudley, A. Forbes, J. Courtial, and M. J. Padgett "Robust interferometer for the routing of light beams carrying orbital angular momentum", *New J. Phys.*, **13** 9, 093014, (2011).
16. G. C. G. Berkhout, M. P. J. Lavery, J. Courtial, M. W. Beijersbergen, and M. J. Padgett, "Efficient Sorting of Orbital Angular Momentum States of Light," *Phys. Rev. Lett.* **105**, 15, 153601 (2010).
17. O. Bryngdahl, "Geometrical transformations in optics," *J. Opt. Soc. Am.* **64**, 8, 1092–1099 (1974).
18. W. Hossack, A. Darling, and A. Dahdour, "Coordinate transformations with multiple computer-generated optical-elements," *J. Mod. Opt.* **34**, 1235–1250 (1987).
19. Y. Saito, S. Komatsu, and H. Ohzu, "Scale and rotation invariant real-time optical correlator using computer generated hologram," *Opt. Comm.* **47**, 1, 8–11 (1983).
20. M. P. J. Lavery, G. C. G. Berkhout, J. Courtial, and M. J. Padgett, "Measurement of the light orbital angular momentum spectrum using an optical geometric transformation," *J. Opt.* **13**, 064006 (2011).
21. G. C. G. Berkhout, M. P. J. Lavery, M. W. Beijersbergen, and M. J. Padgett, "Measuring orbital angular momentum superpositions of light by mode transformation", *Opt. Lett.* **36**, 1863–1865 (2011).
22. J. Wang, J.-Y. Yang, I.M. Fazal, N. Ahmed, Y. Yan, H. Huang, Y. Ren, Y. Yue, S. Dolinar, M. Tur, and A.E. Willner, *Nat. Photon.*, **6** 7, 488496, 2012.
23. C. Paterson, "Atmospheric turbulence and orbital angular momentum of single photons for optical communication", *Phys. Rev. Lett.* **94**, 153901 (2005).
24. M. P. J. Lavery, D. Robertson, G. C. G. Berkhout, G. Love and M. J. Padgett "Refractive elements for the measurement of the orbital angular momentum of a single photon" *Opt. Express*, **20**, 3, (2012).
25. B. Rodenburg, M P. J. Lavery, M Malik, M. N. OSullivan, M. Mirhosseini, D. J. Robertson, M. J. Padgett, and R. W. Boyd, "Influence of atmospheric turbulence on states of light carrying orbital angular momentum", *Opt. Lett.* **37**, 17, 2012.
26. G. A. Tyler and R. W. Boyd, "Influence of atmospheric turbulence on the propagation of quantum states of light carrying orbital angular momentum", *Opt. Lett.* **34**, 142 (2009).
27. D. L. Fried, *J. Opt. Soc. Am.* **55**, 1427 (1965).
28. T.A. Dow, M.H. Miller, P.J. Falter, "Application of a fast tool servo for diamond turning of non-rotationally symmetric surfaces", *J. Precision Eng.* **13**, 243-250 (1991).
29. C. E. Shannon, "A Mathematical Theory of Communication", *Bell Syst. Tech. J.* **27**, 379 (1948).
30. M. J. Padgett and L. Allen, "The Poynting vector in Laguerre-Gaussian laser modes", *Opt. Commun.* **121**, 36 (1995).
31. J. Leach, S. Keen, M. J. Padgett, C. Saunter, and G. D. Love, "Direct measurement of the skew angle of the Poynting vector in a helically phased beam", *Opt. Express* **14** , 11919–11924 (2006).
32. M. P.J. Lavery, D. J. Robertson, A. Sponselli, J. Courtial, N. K. Steinhoff, G. A. Tyler, A. Wilner and M. J. Padgett, "Efficient measurement of orbital angular momentum over 50 different states", submitted to *New J. Phys.* Sep 2012.